

Anomalous Hall conductivity and electronic structures of Si-substituted Mn_2CoAl epitaxial films

K. Arima,¹ F. Kuroda,¹ S. Yamada,^{1,2} T. Fukushima,^{3,4} T. Oguchi,^{2,5,6*} and K. Hamaya^{1,2†}

¹Graduate School of Engineering Science, Osaka University, Toyonaka 560-8531, Japan

²Center for Spintronics Research Network, Osaka University, Toyonaka 560-8531, Japan

³Institute for NanoScience Design, Osaka University, Toyonaka, Osaka 560-8531, Japan

⁴Institute for Dataility Science, Osaka University, Suita, Osaka 565-0871, Japan

⁵Institute of Scientific and Industrial Research, Osaka University, Ibaraki, Osaka 567-0047, Japan and

⁶MI2I, National Institute for Materials Science, Tsukuba 305-0047, Japan

(Dated: June 19, 2019)

We study anomalous Hall conductivity (AHC) and electronic band structures of Si-substituted Mn_2CoAl ($\text{Mn}_2\text{CoAl}_{1-x}\text{Si}_x$). First-principles calculations reveal that the electronic band structure is like a spin-gapless system even after substituting a quaternary element of Si for Al up to $x=0.2$ in $\text{Mn}_2\text{CoAl}_{1-x}\text{Si}_x$. By using molecular beam epitaxy (MBE) techniques, $\text{Mn}_2\text{CoAl}_{1-x}\text{Si}_x$ epitaxial films can be grown, leading to the systematic control of x up to $x=0.3$. Note that a very small AHC of ~ 1.1 S/cm is obtained for $x=0.225$ and the sign of AHC is changed from positive to negative at around $x=0.25$. We discuss the origin of the sign reversal of AHC on the basis of the Fermi level shift in the experimentally obtained MCA.

PACS numbers:

When the conduction and valence band edges meet at the Fermi level and there is no gap for one spin channel while there is a finite gap in another spin channel, these materials are so called spin gapless semiconductors (SGSs).¹⁻³ In the field of spintronics, because the SGSs have intriguing physical properties such as electric-field induced magnetization changes, these materials can be utilized as ferromagnetic semiconductors.⁴ Also, since not only the electrons but also the holes can become fully spin polarized,¹⁻³ one can utilize these materials as highly efficient spin injectors and highly spin polarized channels with tunable magnetic properties.

In recent years, Ouardi *et al.* experimentally demonstrated that an inverse Heusler compound Mn_2CoAl (MCA) shows SGS characteristics such as the vanishing Seebeck effect and positive nonsaturating magnetoresistance with a linear change.⁵ Also, the expected carrier mobility of the MCA bulk has reached ~ 70000 $\text{cm}^2/\text{V}\cdot\text{s}$.⁵ Since the observations of these characteristics, lots of theories and experiments on SGS characteristics of Heusler compounds for both bulk and films have been reported.⁶⁻¹⁶ Unfortunately, for MCA films, there is no report on the vanishing Seebeck coefficient and/or on the positive nonsaturating magnetoresistance.

On the other hand, a very small anomalous Hall conductivity (AHC = σ_{AHC}) has also been considered to be a characteristic of MCA.⁵ With respect to AHC in the MCA bulk,⁵ a small σ_{AHC} of 21.8 S/cm was observed although conventional ferromagnetic Heusler compounds showed relatively large σ_{AHC} of ~ 1000 S/cm.^{17,18} According to Ouardi *et al.*,⁵ a numerical calculation of AHC based on the Berry curvature showed a σ_{AHC} of 3 S/cm,

which was regarded as a consequence of the antisymmetry of the Berry curvature for \mathbf{k}_z vectors of opposite sign. First-principles calculations also revealed an extremely small σ_{AHC} of 0.16 S/cm for ideal (stoichiometric) MCA.¹⁹ Namely, such small σ_{AHC} values are peculiar properties of MCA. Recently, relatively small σ_{AHC} values were shown experimentally even for MCA films.^{12,14-16} In addition, some of studies regarded the small σ_{AHC} as an evidence for the realization of SGS-like MCA.^{14,16} However, the experimentally reported σ_{AHC} values are scattered, and there has so far been no discussion about the correlation between AHC and its electronic structures for MCA films.

In this paper, by intentionally controlling the position of the Fermi level, we study the correlation between AHC and electronic band structures of Si-substituted Mn_2CoAl ($\text{Mn}_2\text{CoAl}_{1-x}\text{Si}_x$) films grown by molecular beam epitaxy (MBE) techniques. First-principles calcu-

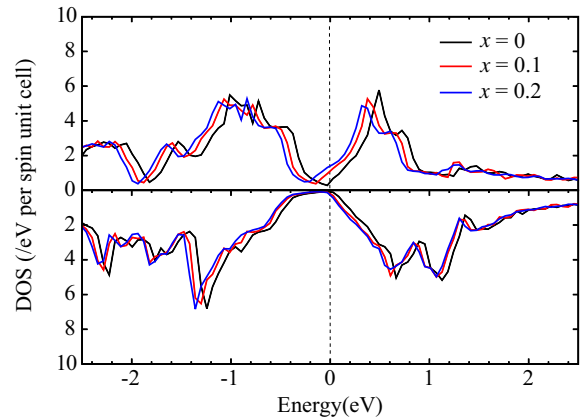


FIG. 1: (Color online) Spin-resolved DOS for the Si-substituted MCA, together with the perfectly ordered MCA.

*E-mail: oguchi@sanken.osaka-u.ac.jp

†E-mail: hamaya@ee.es.osaka-u.ac.jp

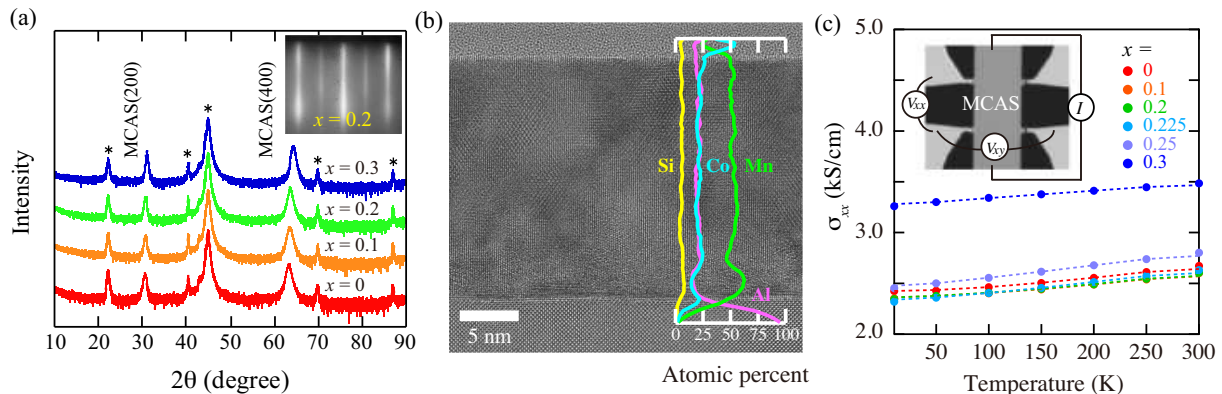


FIG. 2: (Color online) (a) θ - 2θ XRD patterns of the $\text{Mn}_2\text{CoAl}_{1-x}\text{Si}_x$ films. Asterisk marks denoted correspond to the diffraction peaks derived from the $\text{MgAl}_2\text{O}_4(100)$ substrate. The inset shows a RHEED pattern of the surface for $x = 0.2$ during the growth. (b) Cross-sectional TEM image of the $\text{Mn}_2\text{CoAl}_{0.8}\text{Si}_{0.2}$ film, together with the depth profile of the atomic compositions of Mn, Co, Al, and Si. (c) Temperature dependence of σ_{xx} for various $\text{Mn}_2\text{CoAl}_{1-x}\text{Si}_x$ films. The inset shows a fabricated Hall-bar device for transport measurements.

lations reveal that the electronic band structure is like a spin-gapless system at around the Fermi level even after substituting a quaternary element of Si for Al up to $x = 0.2$. We note that a very small σ_{AHC} of ~ 1.1 S/cm can be obtained for $x = 0.225$ and the sign of AHC is changed from positive to negative at around $x = 0.25$. We discuss the origin of the sign change in AHC on the basis of the experimentally obtained MCA.

To elucidate the electronic effect of Si substitution on the electronic structure of MCA, we use the MACHIKANEYAMA2002 program package,²⁰ based on the Korringa-Kohn-Rostoker (KKR) Green's function method.^{21,22} The shape of the crystal potential is approximated with muffin-tin potentials and the angular momentum cutoff (l_{max}) for the Green's function is $l_{\text{max}} = 2$. We employ generalized gradient approximation (GGA)²³ for the exchange-correlation functional. By total energy calculations, the equilibrium lattice constant of MCA is obtained to be 0.578 nm. Si substitution effects are considered within the coherent potential approximation (CPA) to treat the electronic structure and magnetism in disordered systems.^{24,25} The Al sites of MCA are substituted with Si while keeping the lattice constant as pure MCA. In Fig. 1 we calculate spin-resolved density of states (DOS) for the Si-substituted MCA with $x = 0.1$ and 0.2, together with the perfectly ordered MCA ($x = 0$). Even after substituting Si for Al up to $x = 0.2$, the electronic band structure of MCA can be regarded as a SG system having a unique electronic band structure. Note that the Si substitution can shift the position of the Fermi level for investigating AHC in MCA systems.

For exploring magnetotransport properties, $\text{Mn}_2\text{CoAl}_{1-x}\text{Si}_x$ (MCAS) films ($0 \leq x \leq 0.3$) were grown on $\text{MgAl}_2\text{O}_4(100)$ substrates by molecular beam

epitaxy (MBE), where the lattice mismatch between MCA (bulk) and MgAl_2O_4 was $\sim 1.5\%$. After loading the $\text{MgAl}_2\text{O}_4(100)$ substrates into an MBE chamber, we performed a heat treatment at 600 °C for one hour with a base pressure of $\sim 10^{-7}$ Pa. By in-situ reflection high-energy electron diffraction (RHEED) observations, a good surface flatness of the $\text{MgAl}_2\text{O}_4(100)$ substrate was confirmed. Cooling the substrate temperature down to 300 °C, we grew MCAS films with a thickness of ~ 25 nm by co-evaporating Mn, Co, Al and Si using Knudsen cells. Here we used a nonstoichiometric evaporation technique,^{26–28} in which the evaporation ratio of Mn, Co, Al and Si is set to 2 : 0.68 : 2.2 : x for MCAS. As an example, an *in-situ* RHEED pattern for $x = 0.2$ is shown in the inset of Fig. 2(a), indicating good two-dimensional epitaxial growth of the MCAS film.

Figure 2(a) displays θ - 2θ x-ray diffraction (XRD) patterns of the MCAS films for various x . For all the films, (200) and (400) diffraction peaks are clearly observed at 2θ of $\sim 31^\circ$ and 63° , respectively, indicating the formation of $B2$ -ordered Heusler alloys. No diffraction peak derived from the formation of other phases is observed. The estimated lattice constant of the grown MCA ($x = 0$) was ~ 0.587 nm, slightly larger than that of the bulk MCA (~ 0.579 nm)⁵ and the theoretical value (~ 0.578 nm) in our calculations. Because a half of diagonal length of MgAl_2O_4 is 0.5715 nm ($1/\sqrt{2} \times 0.8083$ nm), an in-plane lattice strain can be induced, resulting in an expansion of c -axis lattice constant for MCAS. In Fig. 2(a) we can see the slight shifts of the (200) and (400) diffraction peaks toward higher angles by increasing x , indicating that the c -axis lattice constant is gradually decreased with increasing x . This means the successful substitution of Al for Si in MCAS films.

We further characterized a MCAS film by using cross-sectional transmission electron microscope (TEM) and energy dispersive x-ray spectroscopy (EDX). From the TEM image in Fig. 2(b), we can recognize that the MCAS film for $x = 0.2$ is epitaxially grown on $\text{MgAl}_2\text{O}_4(100)$ with no marked defects and the surface of the MCAS film is very flat. The EDX line profiles of the MCAS/ $\text{MgAl}_2\text{O}_4(100)$ heterostructure are presented in the inset of Fig. 2(b). Even though we co-evaporated Mn, Co, Al and Si with a ratio of 2 : 0.68 : 2.2 : 0.2 for the growth of MCAS ($x = 0.2$), the chemical composition of the MCAS layer along the vertical direction is nearly stoichiometric (Mn : Co : Al : Si = 2 : 1 : 0.8 : 0.2). These features are almost the same as our previous works.^{27,28} For these reasons, the nonstoichiometric MBE technique used here enables us to systematically grow MCAS films on $\text{MgAl}_2\text{O}_4(100)$ with a very flat surface.

To measure electrical and magnetotransport properties, the MCAS films were patterned into Hall-bar devices with $80 \times 80 \mu\text{m}^2$ in size, as shown in the inset of Fig. 2(c), by a conventional photolithography and Ar ion milling technique. Electrical conductivity (σ_{xx}) was measured by a standard dc four-terminal method. Figure 2(c) shows σ_{xx} as a function of the external temperature for various x ($0 \leq x \leq 0.3$). A weak temperature dependence with a slight positive slope of σ_{xx} (semiconducting type), almost equivalent to the bulk MCA reported previously,⁵ is observed for all the x . According to some theoretical calculations,^{29,30} it has been revealed that $L2_1$ -type (Mn-Co-Mn-Al) MCA is a ferromagnetic metal while XA -type (Mn-Mn-Co-Al) MCA shows a SGS. From the results of Fig. 2(c), we can tentatively judge that the predominant structure of the grown MCA and MCAS films is the XA -type structure. In particular, the σ_{xx} value for $x = 0.2$ and 0.225 at 10 K was ~ 2340 S/cm, which is almost equivalent to that for the bulk MCA (~ 2250 S/cm at 10 K).⁵

Hereafter we focus on the anomalous Hall effect of the grown MCAS films. Figure 3(a) shows the field dependent Hall conductivity (σ_{xy}) at 10 K for various MCAS films ($0 \leq x \leq 0.3$). For $x = 0$ (MCA), a relatively small anomalous Hall conductivity (σ_{AHC}) of ~ 8.9 S/cm is obtained, comparable to that for thin-film samples reported elsewhere.^{12,14-16} Thus, we can consider that the electronic band structure of the grown MCA film is similar to that expected from a numerical calculation of σ_{AHC} based on the Berry curvature⁵ or first-principles calculations.¹⁹ With increasing x in Fig. 3(a), σ_{AHC} is gradually decreased and a very small σ_{AHC} of ~ 1.1 S/cm is obtained for $x = 0.225$. We note that a sign reversal of σ_{AHC} from positive to negative can be seen at around $x = 0.25$. For $x = 0.3$, the magnitude of negative σ_{AHC} is further increased. These systematic changes and sign reversal of σ_{AHC} have not been seen yet in MCA systems.

To consider the above unexpected changes of AHC in MCA systems, we firstly check the magnetic properties.

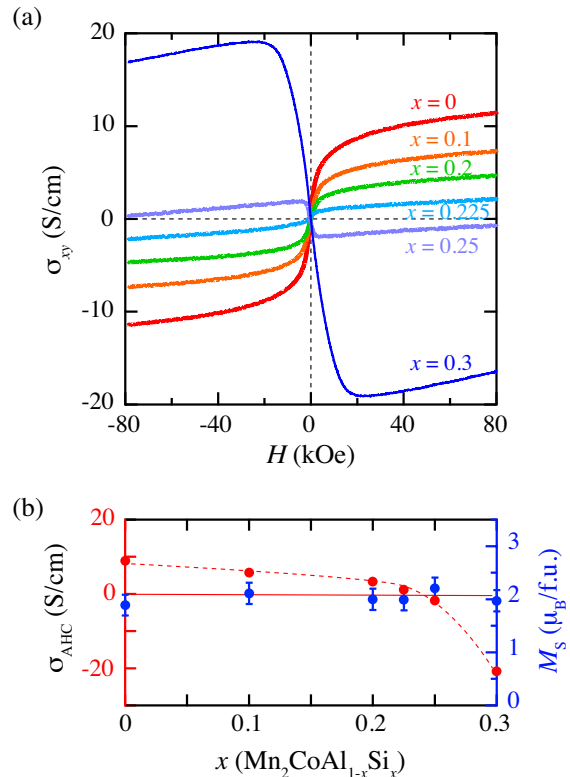


FIG. 3: (Color online) (a) Field-dependent Hall conductivity (σ_{xy}) at 10 K for various MCAS films. (b) σ_{AHC} (left axis) and M_S (right axis) as a function of x at 10 K.

To compare σ_{AHC} with the saturation magnetic moment (M_S) of the MCAS films, we summarize σ_{AHC} (left axis) and M_S (right axis) at 10 K as a function of x in Fig. 3(b). The σ_{AHC} value is largely changed from positive to negative with varying x while the change in M_S is very small. Taking the no correlation between σ_{AHC} and M_S into account, we can infer that the observed anomalous Hall effect in Fig. 3(a) originates from the intrinsic contribution.³¹ One of the origins of the sign reversal of σ_{AHC} will be discussed in the next paragraph. From the slope of the ordinary Hall effect above 50 kOe, the carrier (hole) concentration of our MCAS films can be estimated to be $\sim 10^{22} \text{ cm}^{-3}$. Unfortunately, the carrier concentration is five orders of magnitude larger than that in bulk MCA ($\sim 10^{17} \text{ cm}^{-3}$).⁵ Although the electrical conductivity of our MCAS films showed the semiconducting behavior derived from the XA -type structure, we have to consider the presence of atomic disorders causing the additional carriers in the films. At least, our MCAS films are affected by the lattice strain from the MgAl_2O_4 substrate. If there is the atomic swap between Mn and Al induced by the lattice strain and etc., the SGS behavior cannot be conserved because of the occurrence of the excess DOS in the majority spin band.⁹ Here, using the KKR-CPA calculation, we have already checked that the SGS-like band structure was broken due to the formation of the majority band structure around the Fermi

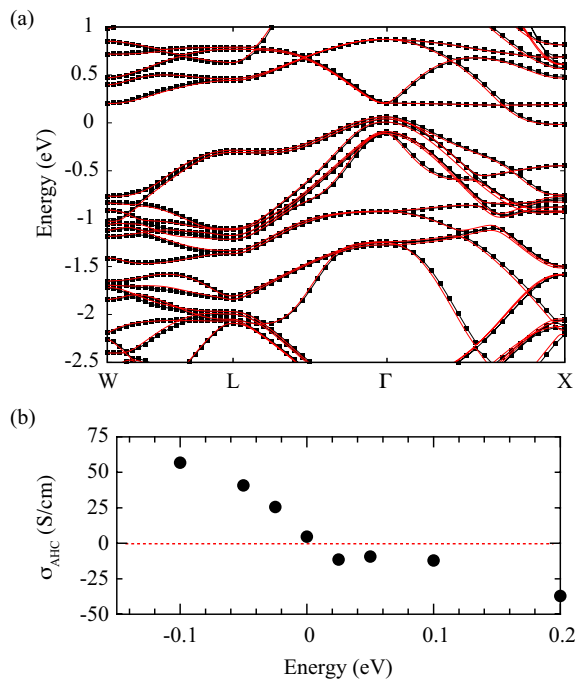


FIG. 4: (Color online) (a) Electronic band structure of MCA. Black dotted and red solid curves are the energy bands obtained from first-principles calculations and Wannier interpolation, respectively. (b) The plot of σ_{AHC} , calculated from the Berry phase approach, versus energy.

level even for MCAS with $x = 0.1$ and 0.2 (not shown here). Although these electronic structures showed half-metals, we should further explore the suppression of the atomic swap between Mn and Al for achieving realistic SGS in the films.

Finally, based on the theory, we discuss an origin of the sign reversal of σ_{AHC} in the epitaxial MCAS films. To calculate σ_{AHC} , the QUANTUM ESPRESSO package³² is used with the relativistic version of the ultrasoft pseudo-potentials using the GGA exchange-correlation functional.²³ The wave vector \mathbf{k} point mesh is taken to be $18 \times 18 \times 18$, and Methfessel-Paxton smearing with a broadening parameter of 0.001 Ry is used. The cutoff energy for the wave function is set to 50 Ry. The tight-binding models are obtained from the first-principles band structure using the Wannier90 program code.³³ For Mn and Co, s , p and d orbitals are adopted to construct the Wannier function. Figure 4(a) displays the calculated electronic band structure of the MCA with

a lattice constant of 0.584 nm, where this value is one of the lattice constant values for a Si substituted MCA film obtained experimentally. We can confirm that the electronic band structure is similar to that of MCA reported in previous works.^{9,34} Obtained tight-binding energy band structure reproduces well the first-principles one as shown in the black dotted curve in Fig. 4(a). σ_{AHC} can be calculated using the tight-binding models with following equation,^{5,35}

$$\sigma_{\text{AHC}} = -\frac{e^2}{h} \int \frac{d\mathbf{k}}{(2\pi)^d} \Omega_z(\mathbf{k}) f(\mathbf{k}), \quad (1)$$

where $\Omega_z(\mathbf{k})$ is the z component of the Berry curvature for \mathbf{k} , $f(\mathbf{k})$ is the Fermi distribution function (at zero Kelvin), and $d = 3$.³⁶ Figure 4(b) shows the calculated result of σ_{AHC} versus energy (E). Here the lattice constant is also assumed to be 0.584 nm, taken from our experimental result. At $E = 0$ (MCA), a σ_{AHC} of ~ 4.6 S/cm is obtained theoretically. We note that the σ_{AHC} value can be varied with shifting the position of E , and the negative σ_{AHC} can be seen. This means that the Fermi level shift induced by the Si substitution in MCA enables the sign reversal of the σ_{AHC} value. Thus, the observed sign reversal of σ_{AHC} , shown in Fig. 3, can roughly be interpreted in terms of the energy shift of the Fermi level in the Si substituted MCA systems. Although we could not demonstrate the MCA film with a SGS band structure experimentally, tuning the position of the Fermi level could be achieved in the MCA films.

In summary, we studied σ_{AHC} and electronic band structures of Si-substituted Mn_2CoAl ($\text{Mn}_2\text{CoAl}_{1-x}\text{Si}_x$). First-principles calculations revealed that the electronic band structure is like a spin-gapless system even after substituting a quaternary element of Si for Al up to $x = 0.2$. Using molecular beam epitaxy (MBE) techniques, we grew $\text{Mn}_2\text{CoAl}_{1-x}\text{Si}_x$ epitaxial films up to $x = 0.3$. For $x \sim 0.225$, a very small σ_{AHC} of ~ 1.1 S/cm was obtained and the sign reversal of σ_{AHC} was seen at around $x = 0.25$. We considered that one of the origins of the sign reversal of σ_{AHC} is the shift of the position of the Fermi level in the experimentally obtained MCA. Further considerations including the atomic swap between Mn and Al will be needed.

This work was partly supported by a Grant-in-Aid for Scientific Research (A) (No. 16H02333) from the Japan Society for the Promotion of Science (JSPS).

¹ X. L. Wang, Phys. Rev. Lett. **100**, 156404 (2008).

² X. L. Wang, S. X. Dou and C Zhang, NPG Asia Materials **2**, 31 (2010).

³ X. Wang, Z. Cheng, J. Wang, X. L. Wang and G. Liu, J. Mater. Chem. C **4**, 7176 (2016).

⁴ H. Ohno, Science **281**, 951 (1998).

⁵ S. Ouardi, G. H. Fecher, C. Felser and J. Kübler. Phys. Rev. Lett. **110**, 100401 (2013)

⁶ S. Skaftouros, K. Özdoğan, E. Sasioglu and I. Galanakis, Appl. Phys. Lett. **102**, 022402 (2013).

⁷ G. Z. Xu, E. K. Liu, Y. Du, G. J. Li, G. D. Liu, W. H. Wang and G. H. Wu, Europhys. Lett. **102**, 17007 (2013).

- ⁸ G. Y. Gao and Kai-Lun Yao, *Appl. Phys. Lett.* **103**, 232409 (2013).
- ⁹ I. Galanakis, K. Özdoğan, E. Sasioglu and S. Blügel, *J. Appl. Phys.* **115**, 093908 (2014).
- ¹⁰ A. Jakobsson, P. Mavropoulos, E. Sasioglu, S. Blügel, M. Lezaic, B. Sanyal and I. Galanakis, *Phys. Rev. B* **91**, 174439 (2015).
- ¹¹ L. Bainsla and K. G. Suresh, *Appl. Phys. Rev.* **3**, 031101 (2016).
- ¹² M. E. Jamer, B. A. Assaf, T. Devakul and D. Heiman, *Appl. Phys. Lett.* **103**, 142403 (2013).
- ¹³ M. E. Jamer, B. A. Assaf, G. E. Sterbinsky, D. A. Arena, and D. Heiman, *J. Appl. Phys.* **116**, 213914 (2014).
- ¹⁴ G. Z. Xu, Y. Du, X. M. Zhang, H. G. Zhang, E. K. Liu, W. H. Wang and G. H. Wu, *Appl. Phys. Lett.* **104**, 242408 (2014).
- ¹⁵ N. Y. Sun, Y. Q. Zhang, H. R. Fu, W. R. Che, C. Y. You, and R. Shan, *AIP Advances* **6**, 015006 (2016).
- ¹⁶ K. Ueda, S. Hirose, and H. Asano, *Appl. Phys. Lett.* **110**, 202405 (2017).
- ¹⁷ D. Bombor, C. G. F. Blum, O. Volkonskiy, S. Rodan, S. Wurmehl, C. Hess and B. Büchner, *Phys. Rev. Lett.* **110**, 066601 (2013).
- ¹⁸ E. Vilanova Vidal, G. Stryganyuk, H. Schneider, C. Felser and G. Jakob, *Appl. Phys. Lett.* **99**, 132509 (2011).
- ¹⁹ J. Kudrnovský, V. Drchal and I. Turek, *Phys. Rev. B* **88**, 014422 (2013).
- ²⁰ H. Akai, *J. Phys. Soc. Jpn.* **51**, 468 (1982).
- ²¹ J. Koringa, *Physica* **13**, 392 (1947).
- ²² W. Kohn and N. Rostoker, *Phys. Rev.* **94**, 1111 (1954).
- ²³ J. P. Perdew, K. Burke, and M. Ernzerhof, *Phys. Rev. Lett.* **77**, 3865 (1996).
- ²⁴ H. Shiba, *Prog.Theor.Phys.* **46**, 77 (1971).
- ²⁵ P. Soven, *Phys. Rev. B* **2**, 4715 (1970).
- ²⁶ K. Hamaya, H. Itoh, O. Nakatsuka, K. Ueda, K. Yamamoto, M. Itakura, T. Taniyama, T. Ono, and M. Miyao, *Phys. Rev. Lett.* **102**, 137204 (2009).
- ²⁷ S. Yamada, K. Tanikawa, S. Oki, M. Kawano, M. Miyao and K. Hamaya, *Appl. Phys. Lett.* **105**, 071601 (2014).
- ²⁸ Y. Fujita, M. Yamada, M. Tsukahara, T. Oka, S. Yamada, T. Kanashima, K. Sawano, and K. Hamaya, *Phys. Rev. Applied* **8**, 014007 (2017).
- ²⁹ H. Luo, Z. Zhu, L. Ma, S. Xu, X. Zhu, C. Jiang, H. Xu and G. Wu, *J. Phys. D: Appl. Phys.* **41**, 055010 (2008).
- ³⁰ Y. Xin, H. Hao, Y. Ma, H. Luo, F. Meng, H. Liu, E. Liu and G. Wu, *Intermetallics* **80**, 10-15 (2017).
- ³¹ N. Nagaosa, J. Sinova, S. Onoda, A. H. MacDonald, and N. P. Ong, *Rev. Mod. Phys.* **82**, 1539 (2010).
- ³² P. Giannozzi *et al.*, *J. Phys.: Condens. Matter.* **21**, 395502 (2009).
- ³³ N. Marzari and D. Vanderbilt, *Phys. Rev. B* **56**, 12847 (1997).
- ³⁴ G. D. Liu, X. F. Dai, H. Y. Liu, J. L. Chen, Y. X. Li, Gang Xiao, and G. H. Wu, *Phys. Rev. B* **77**, 014424 (2008).
- ³⁵ J. Kübler and C. Felser, *Phys. Rev. B* **85**, 012405 (2012).
- ³⁶ X. Wang, J. R. Yates, I. Souza, and D. Vanderbilt, *Phys. Rev. B* **74**, 195118 (2006).